Research Square

Preprints are preliminary reports that have not undergone peer review.
They should not be considered conclusive, used to inform clinical practice,
or referenced by the media as validated information.

Laser Scanning-Based Parameter Extraction for Ship Butt Weld Joints

Yi Shen

shenyi76@just.edu.cn

Jiangsu University of Science and Technology https://orcid.org/0009-0002-3134-2575

Sheng Zhang

Jiangsu University of Science and Technology

Tao Ma

Hunan University

Yuanchao Lin

Jiangsu University of Science and Technology

Lijia Tao

Jiangsu University of Science and Technology

Mingxin Yuan

Jiangsu University of Science and Technology

Research Article

Keywords: ship welding, laser point cloud, butt weld joints, weld parameter extraction, normal vector separation

Posted Date: April 15th, 2026

DOI: https://doi.org/10.21203/rs.3.rs-9257406/v1

License: This work is licensed under a Creative Commons Attribution 4.0 International License. Read Full License

Laser Scanning-Based Parameter Extraction for Ship Butt Weld Joints

Yi Shen [a,c,1], Sheng Zhang [a], Tao Ma [b,d], Yuanchao Lin [a], Lijia Tao [a,c], Mingxin Yuan [a]

a. School of Mechanical Engineering, Jiangsu University of Science and Technology, Zhenjiang, 212100, China

b. College of Electrical and Information Engineering, Hunan University, Changsha, 410082, China

c. Industrial Technology Research Institute (Advanced Metal Materials), Jiangsu University of Science and Technology, Zhangjiagang, 215600, China

d. Jiangsu Automation Research Institute, Lianyungang, 222000, China

Abstract

To address the need for efficient and high-precision extraction of geometric parameters for three types of ship butt welds (I-groove, X-groove, and K-groove), an automatic weld parameter extraction algorithm based on laser scanning is proposed. First, point cloud surface separation is achieved through DBSCAN density clustering for I-groove welds and point cloud normal vector method for X-groove and K-groove welds. Subsequently, a universal parameter extraction module is constructed, incorporating a robust plate thickness calculation method and an adaptive groove angle extraction strategy. Finally, specialized parameter extraction strategies are designed according to the geometric characteristics of each weld type, forming a unified processing framework for multiple types of butt welds. Experimental results demonstrate that the mean absolute errors (MAE) for plate thickness and root gap of I-groove welds are 0.66 mm and 0.58 mm, respectively; the MAE for groove angles of X-groove and K-groove welds is maintained within 4°, while MAE for other parameters is controlled within 1 mm. Comparative experiments show that the proposed algorithm achieves superior measurement accuracy across all three weld types compared to traditional algorithms, with an 81.8% improvement over the slope analysis method, a 73.9% improvement over the height transition feature method, and an overall average accuracy improvement of approximately 77.9%.

Keywords: ship welding; laser point cloud; butt weld joints; weld parameter extraction; normal vector separation

1 Introduction

The harsh welding environment and the urgent need for cost reduction and efficiency improvement in shipyards have driven the rapid development of robotic automated welding technology [1,2]. To enhance welding efficiency and ensure consistency in welding quality, robots typically require precise extraction of weld parameters prior to welding to achieve optimal welding process matching [3,4]. Butt weld joints encompassing I-groove, X-groove, K-groove and other configurations are ubiquitous in ship construction, featuring not only complex groove structures but also frequently coexisting on the same production line. Additionally, noise and occlusion issues during laser scanning pose severe challenges to the accuracy and generality of weld parameter extraction [5]. Therefore, establishing a unified

[1]Corresponding author at: School of Mechanical Engineering, Jiangsu University of Science and Technology, Zhenjiang, 212100, China. E-mail address: shenyi76@just.edu.cn

robust parameter extraction framework to achieve automated and precise measurement of multiple types of ship butt welds has become an urgent requirement for automated ship welding.

In recent years, weld feature measurement technology has experienced rapid development. Regarding weld recognition based on 3D CAD models, Yuan et al. [6] established mathematical models of weld feature parameters based on three types of joint configurations and achieved weld feature parameter extraction according to joint spatial position relationships. For automatic recognition of weld geometric features, Dai et al. [7] performed Delaunay triangular mesh subdivision on 3D models of welded components and identified weld features based on model contours and points after obtaining STL files of the 3D models. Xue et al. [8] proposed a weld feature recognition and parameter extraction method based on feature surface boundaries, which automatically extracted weld feature parameters by extracting corresponding nodes from directed adjacency graphs according to joint types. However, CAD model-based methods rely on the completeness and accuracy of pre-built models. In actual manufacturing, due to assembly errors, thermal deformation and other factors, deviations often exist between models and actual workpiece conditions, making them difficult to meet the requirements of online real-time measurement.

To overcome the limitations of the aforementioned offline modeling methods, online weld geometric parameter measurement methods based on laser vision sensors have experienced rapid development [9]. Addressing the trajectory tracking problem in robotic multi-pass multi-layer welding, Xu et al. [10] proposed an automatic feature point extraction method based on laser vision, achieving precise weld trajectory tracking through laser stripe image processing and improving welding path positioning accuracy. In ship welding automation applications, Baek et al. [11] developed robust laser vision sensing technology, achieving adaptive tracking of butt welds in actual shipyard environments. For V-groove weld starting point positioning, Tang et al. [12] achieved accurate positioning of welding starting points through laser stripe feature analysis. Liao et al. [13] proposed a weld 3D morphological parameter detection method combining vision and structured light, completing parameter extraction based on deep convolution technology. However, the above methods are all based on 2D image processing and mostly rely on manually designed feature extraction rules. They not only fail to completely extract weld parameters due to inability to obtain complete 3D weld information, but also exhibit low parameter extraction efficiency.

To obtain complete 3D geometric information of weld grooves, researchers have begun turning to 3D perception modeling based on laser point clouds. In weld position recognition, Zhou et al. [14] proposed an automatic weld extraction method based on point cloud models for automatic weld path planning problems, achieving automatic weld position recognition through surface segmentation. Li et al. [15] utilized height variation inflection points to extract single-row point cloud features and fit weld trajectories for structural component weld positioning, achieving accurate extraction of H-beam welds. In complex curved surface weld processing, Geng et al. [16] achieved automated welding through surface reconstruction and path optimization based on point cloud-based robotic welding path planning for free-form surface welds such as impeller blades. Yang et al. [17] developed a 3D weld extraction system based on point cloud segmentation for offline programming efficiency issues, achieving automated programming for arc welding robots. Zhang et al. [18] achieved automatic welding trajectory generation through point cloud feature analysis for planar weld scenarios. However, the above methods are mostly designed for specific weld types and lack a unified processing

framework for I-groove, X-groove, K-groove and other butt welds commonly encountered in ship construction. Furthermore, these methods focus on weld trajectory extraction with less attention to weld parameters such as groove angle and root face height that affect welding process matching, which require more refined point cloud segmentation and clustering algorithms.

For precise separation of weld regions in point cloud data, RANSAC and DBSCAN, as two classic point cloud processing algorithms, have been widely applied. In automatic weld region localization, Zhou et al. [19] proposed a DBSCAN-based weld positioning method for weld-base material separation in 3D workpieces, utilizing density clustering characteristics to achieve automatic separation of weld regions from base material surfaces, providing accurate spatial position information for subsequent welding path planning. In complex scene point cloud segmentation, Singh et al. [20] combined RANSAC with clustering methods for 3D point cloud segmentation, achieving satisfactory segmentation results in complex scenarios with noise and occlusion. For high-precision surface extraction requirements, Xie et al. [21] proposed a quadric surface fitting-based 3D point cloud surface segmentation method using DBSCAN clustering, achieving high-precision surface extraction through local quadric surface fitting and density-reachable clustering. Hegedűs-Kuti et al. [22] applied point cloud clustering analysis to welding quality inspection, achieving automatic classification and recognition of welding defects through 3D scanning and point cloud alignment technology. However, in existing research, RANSAC and DBSCAN are mostly used for single plane segmentation or defect detection scenarios, and there is still a lack of differentiated surface separation and parameter extraction strategies for butt welds with different geometric structures such as I-groove, X-groove, and K-groove.

In summary, existing weld parameter extraction methods have the following deficiencies: (1) Methods based on 2D laser stripe images struggle to obtain complete 3D geometric information, with limited measurement accuracy for complex groove structures; (2) Point cloud-based weld extraction methods mostly focus on trajectory planning and are designed for single weld types, lacking parameter extraction for multiple weld types such as I-groove, X-groove, and K-groove; (3) The application of classic point cloud segmentation algorithms such as RANSAC and DBSCAN is still limited to single scenarios, failing to design differentiated surface separation and parameter extraction strategies according to the geometric differences of multiple weld types.

Addressing the above issues, this paper proposes an automatic laser point cloud-based parameter extraction algorithm for ship butt weld joints, achieving high-precision extraction of parameters for three types of welds: I-groove, X-groove, and K-groove. The main contributions are as follows:

(1) A differentiated point cloud surface separation strategy is designed. DBSCAN density clustering is employed for I-groove welds to achieve automatic separation of left and right groove surfaces; a normal vector-based surface separation method is adopted for X-groove and K-groove welds to effectively separate top and side surface point clouds, establishing a reliable data foundation for subsequent parameter extraction.

(2) A universal parameter extraction module is constructed. This module integrates percentile statistics-based plate thickness calculation and endpoint method-based groove angle calculation. Through effective suppression of noise data interference, the universal parameter extraction accuracy for welds with different structures and point cloud densities is improved.

(3) Specialized extraction strategies are designed for the individualized parameters of each butt weld type due to their differentiated structures. For I-groove welds, the root gap is extracted using the shortest Euclidean distance between end faces; for X-groove welds, weld center extraction is achieved through cross-section lowest point localization and local point set mean calculation, and root face height extraction is implemented using sliding window slope peak detection method; for K-groove welds, boundary localization is achieved through global minimum search of scan line y-span distribution curves, and groove length and root face height extraction are completed combining growth threshold determination and local gradient stability detection.

2 Weld Scanning System Overview and Universal Parameter Extraction

2.1 System Overview

Figure 1 illustrates the laser scanning system for ship medium and small assembly welds and the typical geometric characteristics of three types of butt weld joints. To achieve welding process matching for different welds, the gantry-type dual-arm welding robot utilizes its end-mounted laser vision sensor to scan different welds before automatic welding and extract weld parameters through point cloud information, as shown in Figures 1(a) and 1(b). Ship butt weld joints primarily involve three structural configurations: I-groove, X-groove, and K-groove, as illustrated in Figure 1(c). The typical characteristic of I-groove welds is that two plates are butted with parallel end faces without groove machining; X-groove welds feature a double-sided symmetric groove configuration, characterized by V-shaped grooves opened on both upper and lower sides of the plates with an X-shaped cross-section; K-groove welds represent an asymmetric groove configuration, characterized by a groove opened on one side of the plate while the other side maintains a perpendicular end face with a K-shaped cross-section.

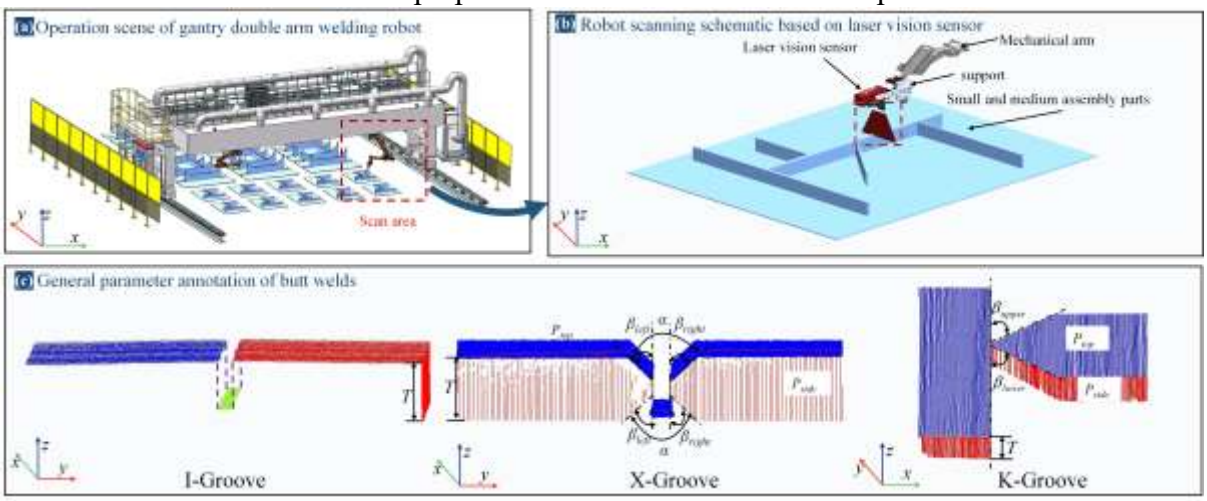


Figure 1 Laser scanning system for ship medium and small assembly welds and weld geometric characteristics: P_{top} represents top surface point cloud; P_{side} represents side surface point cloud; β denotes single groove angle; α denotes total groove angle; T represents plate thickness

To achieve effective and precise extraction of the parameters for the above three types of butt welds, preprocessing is first required to accomplish downsampling and surface separation of the weld point cloud, followed by universal parameter extraction for butt welds and individualized parameter extraction for each weld type.

2.2 Preprocessing of Butt Weld Joints

Since the raw point cloud data acquired by laser scanning is voluminous and contains multiple surface information types, direct processing would compromise algorithm efficiency and accuracy. Therefore, preprocessing is first performed in this study, aimed at reducing data complexity and separating key geometric surfaces, thereby establishing a foundation for subsequent weld feature extraction. Preprocessing mainly comprises two steps: point cloud downsampling and point cloud surface separation, with the latter designed differentially for different weld types. As shown in Figure 1(c), the point cloud acquired by line laser scanning primarily consists of two types: top surface point cloud P_{top} and side surface point cloud P_{side}.

2.2.1 Point Cloud Downsampling

To address the computational burden imposed by excessively high-density raw laser scanning point clouds, this study designs an index-based uniform downsampling method. This method filters the point cloud by setting a fixed step size s, effectively reducing data volume while maximally preserving the spatial uniform distribution characteristics of the point cloud, thereby retaining complete geometric topological structure for subsequent processing.

2.2.2 Point Cloud Surface Separation

For I-groove welds, due to the obvious spatial separation between left and right plates in the y-direction, the DBSCAN algorithm is employed to perform one-dimensional density clustering on y-coordinates to achieve left-right surface separation.

For X-groove and K-groove welds, a normal vector-based surface separation method is adopted. This method fully exploits the significant differences in spatial geometric distribution between top and side surfaces: the top surface region, being approximately horizontally distributed, has a normal vector z-component approaching ±1; while the side surface region, being approximately vertically distributed, has a normal vector z-component approaching 0. Therefore, surface type discrimination is performed by calculating the z-direction unit normal vector $\mathbf{n}_z$ for each point cloud as follows:

$$P = \begin{cases} P_{top} & \text{if} \quad |\mathbf{n}_z| \geq \tau_z \\ P_{side} & \text{otherwise} \end{cases} \tag{1}$$

where τ_z is the z-direction component threshold, set as 0.8 in this study.

2.3 Universal Parameter Extraction for Butt Weld Joints

Upon completion of preprocessing, universal parameter extraction for butt weld joints can be performed. As shown in Figure 1(c), universal parameters include plate thickness T, single groove angle β, and total groove angle α. Since I-groove welds have no groove machining, the groove angle is considered zero; however, to achieve a unified parameter structure for the three weld types, it is still incorporated into the unified framework in the algorithm design.

2.3.1 Plate Thickness Extraction

To avoid the influence of noise such as edge outliers and surface roughness in laser scanning data on plate thickness calculation accuracy, a percentile-based statistical filtering method is adopted to process the plate thickness from the z-coordinates of the side surface point cloud P_{side}:

$$T = P_{99}(\boldsymbol{Z}_{side}) - P_{1}(\boldsymbol{Z}_{side}) \tag{2}$$

where T represents the plate thickness of butt weld joints; $\boldsymbol{Z}_{side}$ denotes the z-coordinate set of all points in the side surface point cloud P_{side}; $P_1(\boldsymbol{Z}_{side})$ and $P_{99}(\boldsymbol{Z}_{side})$ represent the 1st and 99th percentiles, respectively.

This method effectively suppresses the influence of noise on plate thickness extraction parameters by discarding the extreme 1% of isolated data points, thereby improving plate thickness extraction accuracy.

2.3.2 Groove Angle Extraction

For groove angle extraction, the endpoint method is employed, which directly fits a straight line using the starting and ending point coordinates of the groove segment, subsequently calculating the angle between this line and the reference direction.

For any groove segment i ($i \in \{1, 2, 3, 4\}$, representing left, right, upper, and lower groove segments, respectively), given starting point coordinates (x_i^1, y_i^1) and ending point coordinates (x_i^2, y_i^2), the single groove angle β_i is calculated as follows:

$$\beta_i = \arctan\left(\frac{|\Delta y_i|}{|\Delta x_i|}\right) \times \frac{180}{\pi} \tag{3}$$

where $\Delta y_i = |y_i^2 - y_i^1|$ represents the variation in the width direction between the two endpoints of groove segment i; $\Delta x_i = |x_i^2 - x_i^1|$ represents the variation in the weld length direction between the two endpoints.

Subsequently, the total groove angle α_1 for X-groove welds is calculated as:

$$\alpha_1 = \beta_1 + \beta_2 \tag{4}$$

where β_1 and β_2 represent the angles between the left and right groove segments and the vertical direction, respectively.

The total groove angle α_2 for K-groove welds is calculated as:

$$\alpha_2 = \beta_3 + \beta_4 \tag{5}$$

where β_3 and β_4 represent the angles between the upper and lower groove segments and the vertical direction, respectively.

3 Individualized Parameter Extraction for Butt Weld Joints

In addition to the above three universal parameters, each butt weld type possesses individualized weld parameters due to characteristic structural differences, requiring specialized parameter extraction strategies to be designed separately.

3.1 Individualized Parameter Extraction for I-Groove Welds

For I-groove welds, after surface separation, point clouds $P_{left\text{-}I}$ and $P_{right\text{-}I}$ for the left and right plates can be obtained as shown in Figure 2. Therefore, besides the aforementioned universal parameters, I-groove welds also include the root gap g_I.

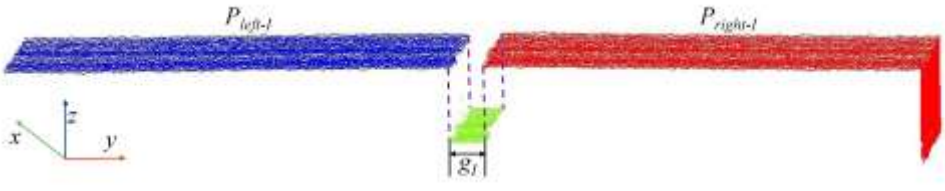


Figure 2 Point cloud geometric characteristics of I-groove welds

The root gap g_I is defined as the shortest Euclidean distance between the two butt end faces:

$$g_I = \mathrm{ABS}(y_{right} - y_{left}) \tag{6}$$

where ABS(·) denotes the absolute value operation; y_{right} represents the minimum y-coordinate in the right point cloud $P_{right\text{-}I}$; y_{left} represents the maximum y-coordinate in the left point cloud $P_{left\text{-}I}$.

3.2 Individualized Parameter Extraction for X-Groove Welds

Compared to I-groove welds, the double-sided symmetric groove structure of X-groove welds makes parameter extraction more complex. After surface separation of X-groove welds, the top surface point cloud $P_{top\text{-}X}$ and side surface point cloud $P_{side\text{-}X}$ can be obtained as shown in Figure 3. Besides universal parameters, X-groove weld parameters also include root face height h_X, and the prerequisite for extracting this parameter is precise determination of the weld center.



Figure 3 Point cloud geometric characteristics of X-groove welds

3.2.1 Weld Center Determination

When extracting the weld center from the top surface point cloud $P_{top\text{-}X}$, irregular regions at the arc starting and ending positions should be avoided to ensure the representativeness of the extracted cross-section. Therefore, the middle position of the point cloud in the x-direction (weld length direction) is selected for cross-sectional analysis. The x-coordinate x_{mid} of this cross-section is:

$$x_{mid} = (x_{max} + x_{min}) / 2 \tag{7}$$

where x_{max} and x_{min} represent the x-direction coordinate values of boundary points on both sides of the top surface point cloud, respectively.

At the cross-section $x = x_{mid}$, the weld center is located at the lowest point of the groove in that cross-section. However, to avoid single-point noise interference, the point cloud set with the minimum z-coordinate and within its δ_z neighborhood on this cross-section is selected, and the weld center position y_c is determined by averaging the y-coordinates of this point cloud set.

3.2.2 Root Face Height Extraction

The root face height exists in the side surface point cloud $P_{side\text{-}X}$. Using the weld center y_c as a reference, the point set $\boldsymbol{P}_{center}$ near the centerline is extracted from the side surface point cloud:

$$\boldsymbol{p}_{center} = \{p_i \in p_{side-X} \mid\mid y_i - y_c \mid < \delta_y\} \tag{8}$$

where δ_y is the y-direction tolerance, set as 2.0 mm in this study.

The centerline point set is sorted by z-coordinate, and local slopes are calculated using a sliding window:

$$k_i = (z_{i+1} - z_i) / (y_{i+1} - y_i) \tag{9}$$

where k_i represents the local slope at the i-th window position; z_i and y_i are the z and y coordinates of the i-th point cloud, respectively.

The characteristic of the root face region is that its slope absolute value in the z-direction is significantly greater than that of the groove region (approaching vertical). The root face is located by detecting peak positions in the slope sequence. Given the slope absolute value sequence $\boldsymbol{S} = \{|s_1|, |s_2|, \ldots, |s_n|\}$, the peak index k_{peak} is calculated as:

$$k_{peak} = \arg\max(\boldsymbol{S}) \tag{10}$$

where argmax(·) denotes the index corresponding to the maximum value element in $\boldsymbol{S}$.

If this peak satisfies the significance condition:

$$s_{k_{peak}} > 2\sigma_s \tag{11}$$

where σ_s is the standard deviation of the slope absolute value sequence $\boldsymbol{S}$.

Then the index k_{peak} corresponds to the boundary position of the root face region. Accordingly, the root face height h_X for X-groove welds can be further calculated as:

$$h_X = | z_{top} - z_{bottom} | \tag{12}$$

where z_{top} and z_{bottom} represent the z-coordinates of the upper and lower boundaries of the root face region, respectively.

3.3 Individualized Parameter Extraction for K-Groove Welds

As an asymmetric groove configuration, K-groove welds share both commonalities and differences with X-groove welds in parameter extraction methods. After surface separation of K-groove welds, the top surface point cloud $P_{top\text{-}K}$ and side surface point cloud $P_{side\text{-}K}$ are obtained. Besides universal parameters, K-groove welds also include individualized parameters as shown in Figure 4: upper groove length L_{upper_K}, lower groove length L_{lower_K}, and root face height h_K. Left boundary localization is required before parameter extraction.

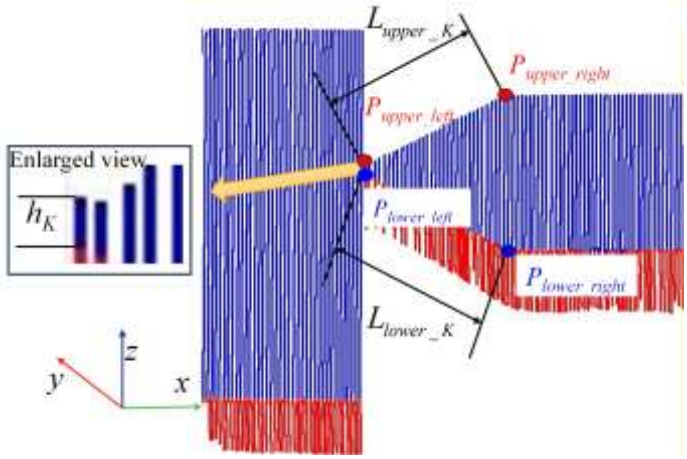


Figure 4 Point cloud geometric characteristics of K-groove welds

3.3.1 Left Boundary Localization

To precisely locate the left boundary of the K-groove weld, a tolerance-based grouping strategy is designed based on the column-by-column laser scanning method along the x-direction. If the following equation is satisfied, two point clouds are grouped into the same scan line; otherwise, the grouping tolerance is reset and new judgment continues:

$$| x_{i+1} - x_i | < \delta_x \tag{13}$$

where x_i *and* x_{i+1} are the x-coordinates of two adjacent points; δ_x is the grouping tolerance.

For the j-th scan line, the y-direction distribution range is calculated as:

$$\Delta y_j = y_{max}^j - y_{min}^j \tag{14}$$

where y_{max}^j and y_{min}^j represent the maximum and minimum y-coordinates of all points on the j-th scan line, respectively.

Thus, a y-direction distribution range curve $\boldsymbol{D}_r = \{\Delta y_1, \Delta y_2, \ldots, \Delta y_n\}$ is constructed. For K-groove welds, the left boundary is an ungrooved vertical segment connecting the upper groove and lower end face, geometrically manifested as the scan line y-span contracting to a minimum at this position. The global minimum position is searched in $\boldsymbol{D}_r$:

$$j^* = \arg\min(\boldsymbol{D}_r) \tag{15}$$

where j* is the index corresponding to the minimum value element in $\boldsymbol{D}_r$, and its corresponding x-coordinate $x_{left\text{-}K}$ is the x-position of the left boundary.

Then the corresponding maximum y-value at this position is the y-coordinate y_{upper_left} of the upper-left boundary, and the corresponding minimum y-value is the y-coordinate y_{lower_left} of the lower-left boundary.

3.3.2 Groove Right Boundary Localization and Parameter Extraction

Starting from the left boundary, the right boundary is searched toward the right side. First, a growth threshold τ_g is defined:

$$\tau_g = \overline{\Delta y} + \sigma_{\Delta y} \tag{16}$$

where $\overline{\Delta y}$ is the mean of all scan line y-spans; $\sigma_{\Delta y}$ is their standard deviation.

Starting from the left boundary index j*, a search sequence toward the right is constructed as $\boldsymbol{S}_{right} = \{j^*+1, j^*+2, \ldots, n\}$. For each index j in the search sequence, the following determination is executed:

(1) If $\Delta y_j > \tau_g$, mark entry into the growth phase;

(2) Calculate local gradient $\Delta j = \Delta y_{j+1} - \Delta y_j$. If $|\Delta_j| < 0.5$ mm and the future window is stable, determine this position as the boundary.

Thus, the right boundary index j_{right} is obtained, with corresponding x-coordinate x_{right_K}. Then the corresponding maximum y-value at this position is the y-coordinate y_{upper_right} of the upper-right boundary, and the corresponding minimum y-value is the y-coordinate y_{lower_right} of the lower-right boundary.

After completing boundary localization, groove length and root face height can be calculated based on the coordinates of each boundary point. The groove length is determined by the Euclidean distance between endpoints of each segment:

$$L_{upper_K} = \sqrt{(y_{upper_right} - y_{upper_left})^2 + (x_{right_K} - x_{left_K})^2} \tag{17}$$

$$L_{lower_K} = \sqrt{(y_{lower_right} - y_{lower_left})^2 + (x_{right_K} - x_{left_K})^2} \tag{18}$$

The root face height h_K is defined as the y-coordinate difference between the upper and lower groove segments at the root face:

$$h_K = | y_{upper_left} - y_{lower_left} | \quad (19)$$

4 Experimental Verification and Analysis

4.1 Experimental Design and Data Acquisition

4.1.1 Experimental Platform

To validate the effectiveness of the proposed weld parameter extraction algorithm, a point cloud acquisition system based on laser vision sensors was established. As shown in Figure 5, the experimental platform primarily consists of a laser vision sensor, collaborative robot, welding specimens, welding torch, and Intel NUC mini host computer.

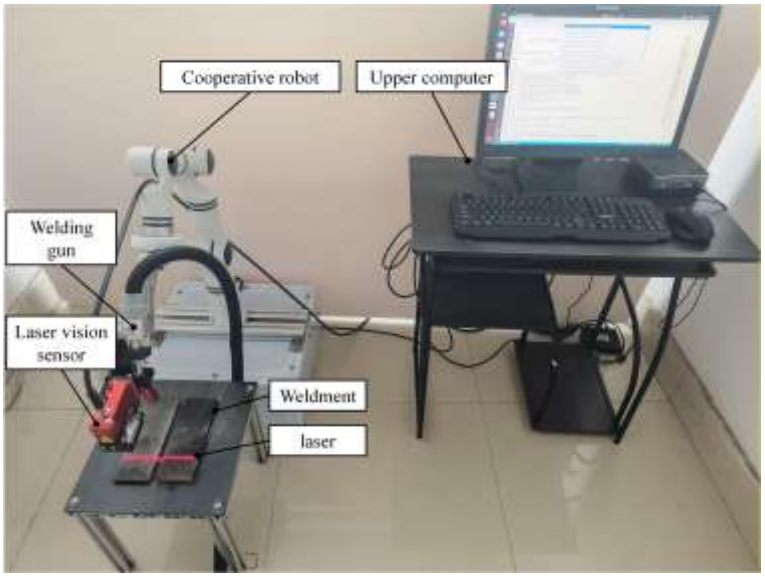


Figure 5 Laser scanning experimental platform

The laser vision sensor adopts the Mingtu CP160V model, with main technical parameters listed in Table 1. This sensor possesses high precision, large measurement range, and excellent anti-interference capability, making it suitable for three-dimensional reconstruction tasks in welding scenarios.

Table 1 Technical parameters of laser vision sensor

Parameter Name	Value	Unit
Scanning frequency	115	HZ
Near-end viewing distance	80	mm
Far-end viewing distance	240	mm
Near-end laser width	56.5	mm
Far-end laser width	134	mm
Linear accuracy	±0.1	mm

The collaborative robot (Model: RealMan RM65_B) is used to drive the laser sensor for uniform-speed scanning along the weld direction. The robot's repeated positioning accuracy is ±0.05 mm, ensuring the stability and consistency of the scanning path. The scanning speed is set at 20 mm/s to ensure that the point cloud density meets the accuracy requirements for parameter extraction.

4.1.2 Data Acquisition and Preprocessing

Three types of typical weld butt joint specimens—I-groove, X-groove, and K-groove—

were fabricated in this study using Q235B low-carbon steel as the material. Five groups of I-groove weld specimens with different parameters were prepared to verify the algorithm's applicability under various geometric parameters; two groups of typical specimens each were prepared for X-groove and K-groove welds for algorithm validation. Table 2 lists the parameter ranges covered by the specimens.

Table 2 Design parameters of weld specimens

Weld Type	Plate Thickness (mm)	Groove Angle (°)	Root Gap (mm)
I-groove	4-13	-	3-12
X-groove	7-10	30-60	-
K-groove	20-40	30-65	-

To acquire three-dimensional point cloud information of the key geometric structures of the weldments, the collaborative robot was utilized to drive the laser vision sensor to perform multi-surface scanning of the weldments. As shown in Figure 6, the line laser vision sensor acquires two-dimensional cross-sectional information of the current scanning section and outputs the vertical distance Δz (corresponding to point cloud z-coordinate) and lateral position Δy (corresponding to point cloud y-coordinate) in the sensor coordinate system. Using the base coordinate system as the global reference, the robot controls the sensor to advance in the negative direction of the x_0 axis with a step displacement $\Delta x'$ and records the starting position Δx; thus, the x-coordinate of each point cloud frame is $\Delta x + \Sigma\Delta x'$. By combining the x, y, z coordinate information of each frame, the complete three-dimensional point cloud structure of the weldment is generated through accumulation and stitching.

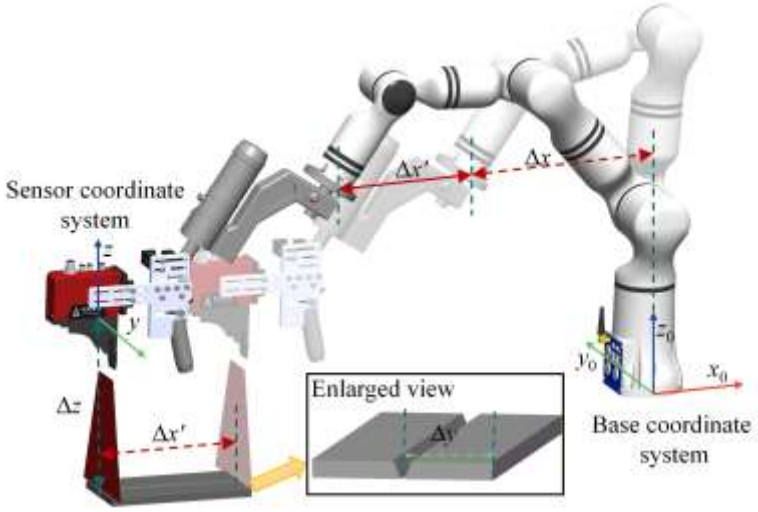


Figure 6 Schematic diagram of weldment scanning coordinate system

Based on the above three-dimensional point cloud construction method, two typical surfaces of the weldments were selected for laser scanning in the experiment, and point clouds in different coordinate systems were aligned and unified for processing. To maintain the original authenticity of the data, no filtering was performed on the raw point clouds. Based on this acquisition and processing workflow, point cloud data for 9 groups of welding specimens were obtained.

4.2 Parameter Extraction Accuracy Verification

To quantitatively evaluate the parameter measurement accuracy of each algorithm, Mean

Absolute Error (MAE) and Mean Relative Error (MRE) are adopted as accuracy evaluation metrics, as shown in Equations (20) and (21):

$$\mathrm{MAE} = \frac{1}{n}\sum_{i=1}^{n} | y_i^{pred} - y_i^{true} | \tag{20}$$

$$\mathrm{MRE} = \frac{1}{n}\sum_{i=1}^{n} \frac{| y_i^{pred} - y_i^{true} |}{y_i^{true}} \times 100\% \tag{21}$$

where y_i^{pred} represents the predicted value; y_i^{true} represents the true value; n is the number of samples. A smaller MAE value indicates higher detection accuracy, while MRE reflects the average proportion of error relative to the true value.

4.2.1 I-Groove Weld Parameter Extraction Results

As a fundamental welding joint configuration, I-groove weld parameter extraction primarily focuses on two key geometric features: plate thickness and root gap. The experiment verified five groups of I-groove weld samples with different parameters, with accuracy statistics shown in Table 3.

Table 3 Accuracy statistics of I-groove weld parameter extraction

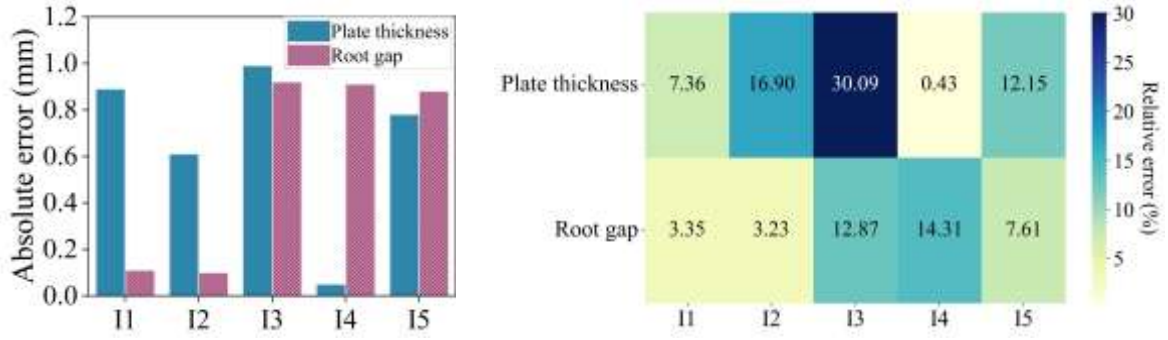
Parameter Name	MAE	RMSE	Maximum Error	RE/%
Plate thickness (mm)	0.66	0.70	0.99	13.39
Root gap (mm)	0.58	0.70	0.92	8.27

The experimental results demonstrate that the extraction accuracy for both plate thickness and root gap of I-groove welds is high, with MAE values of 0.66 mm and 0.58 mm, respectively, and maximum errors controlled within 1 mm. The high precision of plate thickness measurement primarily benefits from the effective suppression of outliers by the percentile-based statistical filtering method. The measurement accuracy of root gap is slightly superior to that of plate thickness, with RE of only 8.27%, because the end face, as a distinct geometric boundary feature, possesses good discriminability in the point cloud.

Figure 7 displays the absolute error distribution and relative error heatmap for plate thickness and gap of the five samples. The experimental results show that the absolute errors of plate thickness for the five samples exhibit certain fluctuations, with error ranges between 0.05-0.99 mm. Sample I4 has the smallest plate thickness error, while sample I3 has the largest. The main reason for this difference lies in the influence of plate thickness dimensions on point cloud quality: Sample I4 has a plate thickness of 11.50 mm, with the plate side having sufficient scanning height and uniform point cloud distribution, enabling the percentile-based statistical filtering method to obtain stable boundary estimates; Sample I3 has a plate thickness of only 3.29 mm, with limited side surface point cloud quantity, resulting in a relatively increased proportion of edge outliers in the total point count, reducing the stability of statistical filtering method estimation. The absolute error distribution for gap measurement ranges between 0.10-0.92 mm. Samples I1 and I2 have relatively small gap errors, with true gaps of 3.28 mm and 3.10 mm, respectively; samples I3-I5 have larger gap errors, with true gaps in the 6-12 mm range.

From the relative error heatmap, it can be observed that plate thickness and gap exhibit different relative error distribution characteristics. The inter-sample variation in plate thickness relative error is significant: Sample I3 reaches 30.09%, while Sample I4 is only 0.43%. This difference stems from the computational characteristics of relative error: the absolute error of

Sample I3 (0.99 mm) is amplified relative to its smaller plate thickness reference (3.29 mm), whereas the absolute error of Sample I4 (0.05 mm) is diminished relative to its larger plate thickness reference (11.50 mm). The relative error distribution of gap is relatively uniform, with all five samples within the 3.23%-14.31% range, indicating good adaptability of the I-groove weld root gap extraction method to gaps of different scales.



(a) Absolute error distribution (b) Relative error heatmap

Figure 7 I-groove weld parameter extraction errors

4.2.2 X-Groove Weld Parameter Extraction Results

As a double-sided symmetric groove structure, X-groove welds involve six parameters: four groove angles (upper and lower), root face height, and plate thickness. The experiment conducted parameter extraction on two groups of X-groove weld samples, with accuracy statistics shown in Table 4.

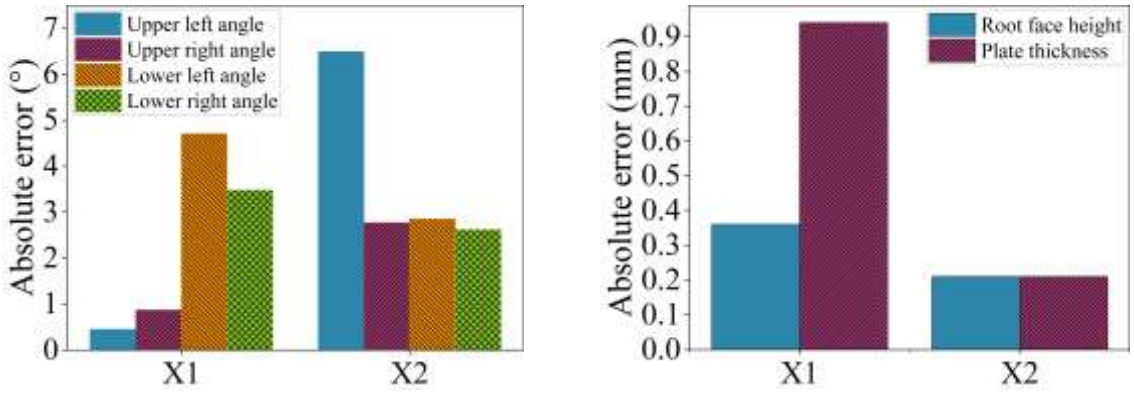
Table 4 Accuracy statistics of X-groove weld parameter extraction

Parameter Name	MAE	RMSE	Maximum Error	RE/%
Upper groove left angle (°)	3.47	4.60	6.49	3.57
Upper groove right angle (°)	1.82	2.05	2.77	1.67
Lower groove left angle (°)	3.78	3.89	4.71	4.96
Lower groove right angle (°)	3.05	3.08	3.48	3.56
Root face height (mm)	0.29	0.29	0.36	14.32
Plate thickness (mm)	0.58	0.68	0.94	3.06

The experimental results show that there are significant differences in MAE among the four groove angles, with the upper groove right angle achieving the highest accuracy (MAE = 1.82°), while the lower groove left angle and upper groove left angle have MAE values of 3.78° and 3.47°, respectively. This difference mainly stems from two factors: first, the occlusion effect of laser scanning—the lower surface point cloud density is only 60%–70% of the upper surface, leading to incomplete geometric features; second, the boundary clarity differs between left and right grooves—the right groove has a smoother transition with the top surface and more stable normal vector gradient variation, facilitating boundary identification; whereas the left groove boundary exhibits more local fluctuations and noise, increasing positional increments. The MAE of root face height is 0.29 mm with a relative error of 14.32%, because the X-type structure has grooves on both sides of the root face, requiring simultaneous identification of upper and lower inflection points during gradient analysis, increasing detection difficulty. Plate thickness measurement is unaffected by grooves and is directly calculated from side surface point clouds through the percentile statistical filtering method, with an MAE of 0.58 mm and relative error of only 3.06%.

Figure 8 displays the absolute error distribution for each parameter of X-groove welds.

The experimental results show that samples X1 and X2 exhibit different error distributions across the four groove angles. Sample X1 has smaller errors in upper grooves but larger errors in lower grooves; Sample X2 has larger errors in the upper groove left angle while lower groove errors are relatively balanced. This difference mainly stems from sample point cloud quality: Sample X1 has a smooth upper groove surface with machining textures on the lower groove; Sample X2 has local depressions on the upper left groove side, affecting linear fitting accuracy. Both root face height error and plate thickness error of Sample X1 are greater than those of Sample X2. The lower root face detection accuracy of Sample X1 is due to the larger difference between its upper and lower groove angles, resulting in more complex geometric transitions in the root face region, increasing the difficulty of inflection point localization.



(a) Groove angles (b) Root face height and plate thickness

Figure 8 X-groove weld absolute error distribution

Figure 9 displays the relative error distribution for each parameter of X-groove welds in heatmap format. The experimental results show that the relative error of root face height is most significant, reaching 26.09% and 34.43% for samples X1 and X2, respectively. This is because the root face dimension itself is small (0.61–1.38 mm), and absolute errors around 0.3 mm are amplified in relative metrics. The relative error of the upper groove left angle in Sample X2 is 13.84%. The relative errors of other parameters are basically controlled within 10%.

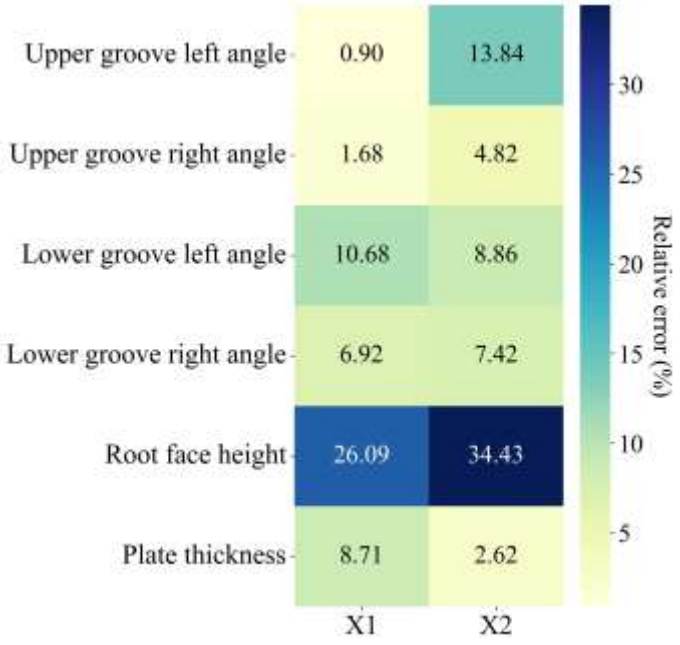


Figure 9 X-groove weld relative error heatmap

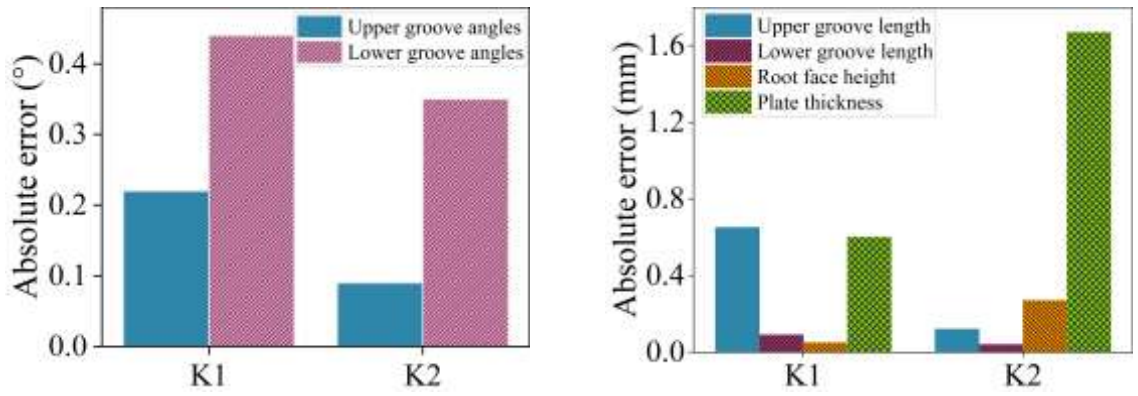
4.2.3 K-Groove Weld Parameter Extraction Results

K-groove welds represent the most complex asymmetric groove configuration, involving six parameters: upper and lower groove angles, upper and lower groove lengths, root face height, and plate thickness. The experiment conducted parameter extraction on two groups of K-groove weld samples, with accuracy statistics shown in Table 5.

Table 5 Accuracy statistics of K-groove weld parameter extraction

Parameter Name	MAE	RMSE	Maximum Error	RE/%
Upper groove angle (°)	0.16	0.17	0.22	0.13
Lower groove angle (°)	0.40	0.39	0.44	0.31
Upper groove length (mm)	0.39	0.47	0.65	0.50
Lower groove length (mm)	0.07	0.07	0.09	0.08
Root face height (mm)	0.16	0.19	0.27	3.01
Plate thickness (mm)	1.14	1.25	1.67	2.01

The experimental results demonstrate that as the most complex multi-layer structure, K-groove welds exhibit significant differences in extraction accuracy across parameters. Groove angle measurement accuracy performs excellently, with MAE values of 0.16° and 0.40° for upper and lower groove angles, respectively, achieving sub-degree precision. This benefits from the scan line analysis-based left-right boundary localization strategy, which effectively identifies the transition boundaries between K-groove grooves and planes through dual criteria of growth phase detection and gradient stabilization. Regarding groove length, the MAE of lower groove length is only 0.07 mm with a relative error of 0.08%, demonstrating extremely stable performance. The MAE of upper groove length is 0.39 mm with a relative error of 0.50%, which remains within an acceptable range for groove lengths of 30-40 mm. The MAE of root face height is 0.16 mm with a relative error of 3.01%. The MAE of plate thickness measurement is 1.14 mm with a relative error of 2.01%, slightly higher than other weld types. This is mainly because the frontal scanning configuration of K-groove welds results in relatively low side surface point cloud density, and the lower end face is occluded by support structures, leading to sparse bottom point clouds, increasing the deviation of the percentile-based statistical filtering method. Nevertheless, for plate thicknesses of 24-34 mm, this accuracy remains within the engineering acceptable range. Overall, K-groove welds achieve sub-degree angle precision and sub-millimeter length precision, fully validating the effectiveness of the scan line analysis-based boundary recognition algorithm for complex multi-layer structures.



(a) Groove angles

(b) Groove lengths, root face height, and plate thickness

Figure 10 K-groove weld absolute error distribution

Figure 10 displays the absolute error distribution for each parameter of K-groove welds. The experimental results show that both samples exhibit low levels of groove angle errors. Sample K2 has slightly better accuracy than Sample K1, which is related to groove angle magnitude: Sample K2's groove angles (approximately 61°-64°) are slightly larger than Sample K1's (approximately 60°-62°), and larger groove angles result in increased projection area of groove surfaces in the point cloud, making geometric features more prominent and facilitating boundary identification and angle calculation. Regarding groove length, the larger error in Sample K1 is due to slight machining burrs at the upper groove boundary, affecting boundary point localization accuracy. The larger plate thickness error in Sample K2 is because the lower end face occlusion is more severe during scanning, degrading bottom point cloud quality.

Figure 11 displays the relative error distribution for each parameter of K-groove welds in heatmap format. The experimental results show that K-groove welds overall exhibit light tones, with most parameters having relative errors at low levels. The relative errors of groove angles and groove lengths are concentrated in the 0.1%–1.8% range. The relative error of root face height in Sample K2 is 11.34%. The relative error of plate thickness in Sample K2 is 7.48%, still controlled within 10%.

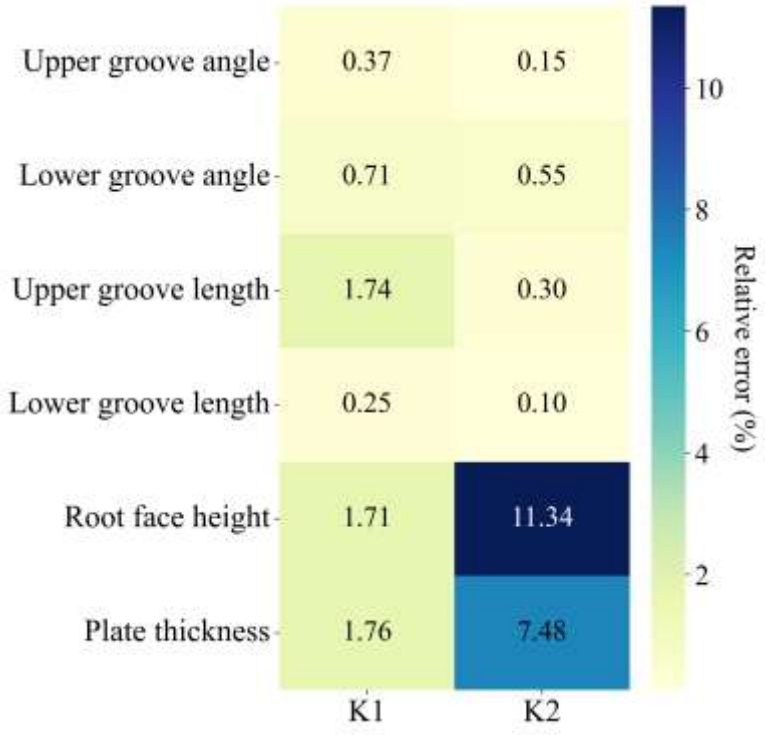


Figure 11 K-groove weld relative error heatmap

4.3 Algorithm Comparison Experiments

4.3.1 Comparison Algorithms and Experimental Setup

To comprehensively evaluate the performance advantages of the proposed algorithm, two representative algorithms are selected for comparison: the traditional slope analysis method [12] and the height analysis with RANSAC fitting method (height transition feature method) [15]. The slope analysis method identifies geometric features by calculating the local slope of point cloud height variations—simple to implement but sensitive to noise; the height transition feature method utilizes RANSAC fitting to suppress outlier influence, offering better robustness than the slope analysis method, but its global height statistics-based layering

strategy struggles to handle multi-level geometric structures. All three algorithms run on the same raw point cloud data without additional preprocessing or filtering operations, and quantitative evaluation is conducted using mean absolute error (MAE) as the core evaluation metric.

4.3.2 I-Groove Weld Comparison Results

Table 6 presents the MAE comparison results of the three algorithms on I-groove welds.

Table 6 MAE comparison of different algorithms on I-groove welds

Parameter Name	Slope Analysis Method	Height Transition Feature Method	Proposed Algorithm
Plate thickness (mm)	1.49	1.30	0.66
Root gap (mm)	1.10	0.68	0.58

From Table 6, it can be observed that the proposed algorithm achieves a plate thickness MAE of 0.66 mm, representing a 55.7% reduction compared to the slope analysis method and a 49.2% reduction compared to the height transition feature method; the root gap MAE is 0.58 mm, representing a 47.3% reduction compared to the slope analysis method and a 14.7% reduction compared to the height transition feature method.

Figure 12 further reveals the performance differences of the three algorithms across individual samples. The error curve of the slope analysis method exhibits the largest fluctuations, demonstrating poor adaptability to thin plate and large gap samples. The error curve of the height transition feature method is relatively stable but maintains an overall level higher than the proposed algorithm. The proposed algorithm maintains the lowest errors across all five samples with minimal inter-sample fluctuations, indicating that the percentile-based statistical filtering method possesses stable adaptability to different geometric parameter configurations.

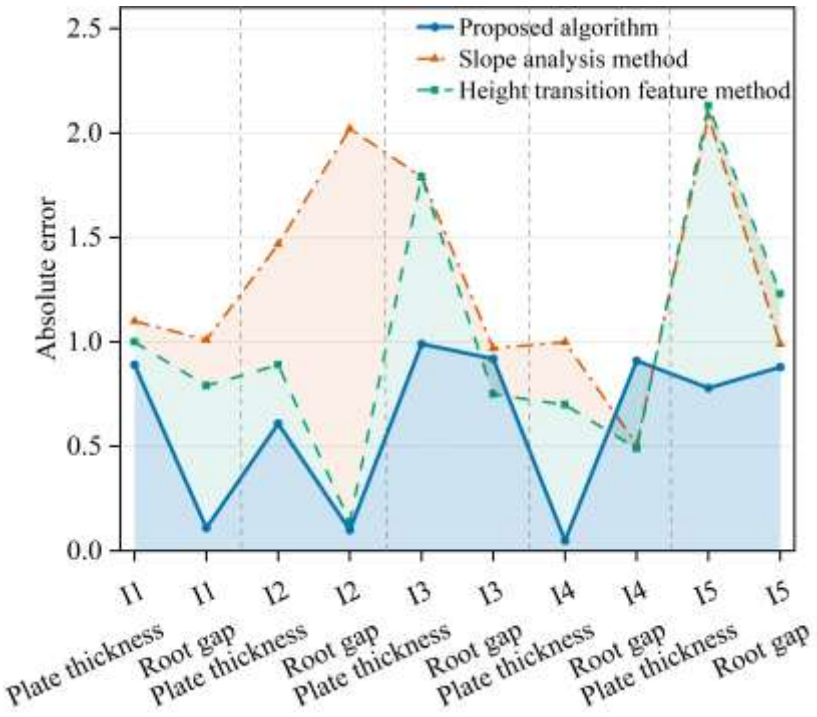


Figure 12 Error comparison of three algorithms on I-groove welds

4.3.3 X-Groove Weld Comparison Results

Table 7 presents the MAE comparison results of the three algorithms on X-groove welds.

Table 7 Accuracy comparison of different algorithms on X-groove welds

Parameter Name	Slope Analysis Method	Height Transition Feature Method	Proposed Algorithm
Upper groove left angle (°)	6.40	6.40	3.47
Upper groove right angle (°)	8.63	5.67	1.82
Lower groove left angle (°)	13.60	4.91	3.78
Lower groove right angle (°)	16.38	4.21	3.05
Root face height (mm)	0.67	0.61	0.29
Plate thickness (mm)	3.43	3.43	0.58

The double-sided symmetric structure of X-groove welds significantly increases parameter extraction difficulty, and the performance gap among the three algorithms widens further on this weld type. From Table 7, it can be observed that the slope analysis method exhibits severe degradation in lower groove angle measurement, with MAE reaching 13.60°-16.38°; the height transition feature method performs better than the slope analysis method, but lower groove angle MAE still remains in the 4°-5° range; the proposed algorithm maintains all four groove angle MAE values within 4°, with plate thickness MAE of 0.58 mm, representing an 83.1% reduction compared to the comparison methods.

Figure 13 clearly displays the performance stratification of the three algorithms. The error curve of the slope analysis method rises sharply for lower groove parameters, indicating that this method cannot effectively handle point cloud occlusion issues arising from double-sided scanning. The error curve of the height transition feature method is relatively stable but still exhibits fluctuations at the transition positions between upper and lower grooves. The proposed algorithm maintains stable low error levels across all samples, validating its effectiveness for double-sided structures.

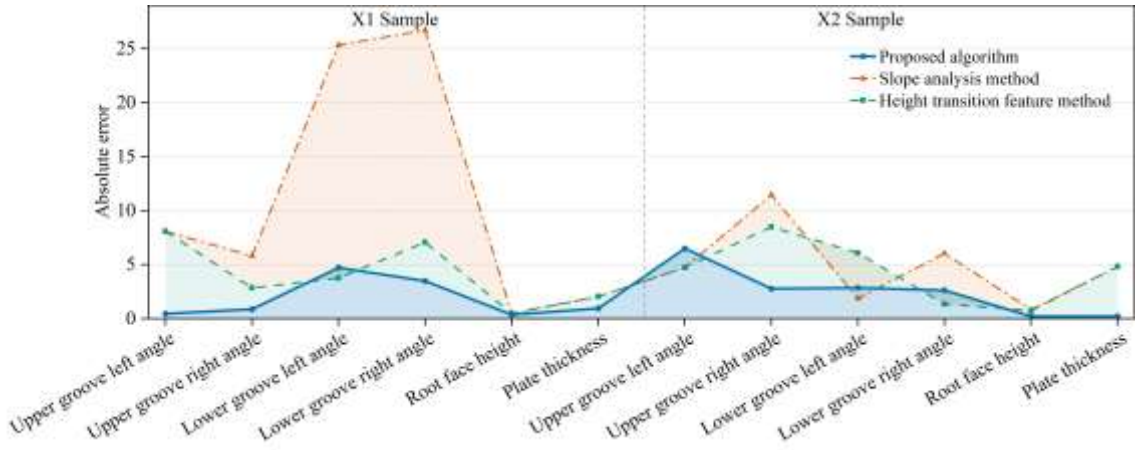


Figure 13 Error comparison of three algorithms on X-groove welds

4.3.4 K-Groove Weld Comparison Results

Table 8 presents the MAE comparison results of the three algorithms on K-groove welds.

Table 8 Accuracy comparison of different algorithms on K-groove welds

Parameter Name	Slope Analysis Method	Height Transition Feature Method	Proposed Algorithm
Upper groove angle (°)	13.86	11.62	0.16
Lower groove angle (°)	10.15	3.66	0.40
Upper groove length (mm)	5.46	9.72	0.39

Continuation Table

Parameter Name	Slope Analysis Method	Height Transition Feature Method	Proposed Algorithm
Lower groove length (mm)	3.41	5.13	0.07
Root face height (mm)	0.40	0.28	0.16
Plate thickness (mm)	5.65	5.65	1.14

The experimental results demonstrate that for K-groove welds, as the most structurally complex asymmetric multi-layer welds, both comparison algorithms exhibit significant measurement accuracy decline, while the proposed algorithm maintains high accuracy, showing remarkable advantages. In terms of groove angles, the proposed algorithm achieves mean absolute errors of 0.16° and 0.40° for upper and lower groove angles, respectively, realizing sub-degree measurement precision. Compared to the slope analysis method, the proposed algorithm achieves accuracy improvements of 98.85% and 96.06% for upper and lower groove angle measurements, respectively; compared to the height transition feature method, accuracy improvements of 98.62% and 89.07%, respectively; overall accuracy improvement ranges from 89.07% to 98.85%. In terms of groove length, the proposed algorithm achieves MAE values of 0.39 mm and 0.07 mm for upper and lower groove lengths, respectively. Compared to the slope analysis method, the proposed algorithm achieves accuracy improvements of 92.86% and 97.95% for groove length measurements, respectively; compared to the height transition feature method, accuracy improvements of 95.99% and 98.64%, respectively; overall accuracy improvement ranges from 92.86% to 98.64%. For root face height, the proposed algorithm achieves an MAE of 0.16 mm, representing a 60.00% accuracy improvement compared to the slope analysis method and a 42.86% improvement compared to the height transition feature method. In plate thickness measurement, both the slope analysis method and height transition feature method achieve MAE of 5.65 mm, while the proposed algorithm reduces the error to 1.14 mm, representing a 79.82% accuracy improvement compared to both comparison algorithms.

Figure 14 intuitively presents the performance gap among the three algorithms on K-groove welds. The error curves of the slope analysis method and height transition feature method maintain high levels across multiple parameters, with particularly severe fluctuations in groove angle and length measurements. This indicates that the global height statistics-based layering strategy struggles to adapt to the complex multi-layer structure of K-groove welds. The error curves of the proposed algorithm closely approach the zero line across all parameters, with extremely high consistency between the two samples, validating the strong adaptability of the scan line analysis-based boundary recognition strategy to complex structures.

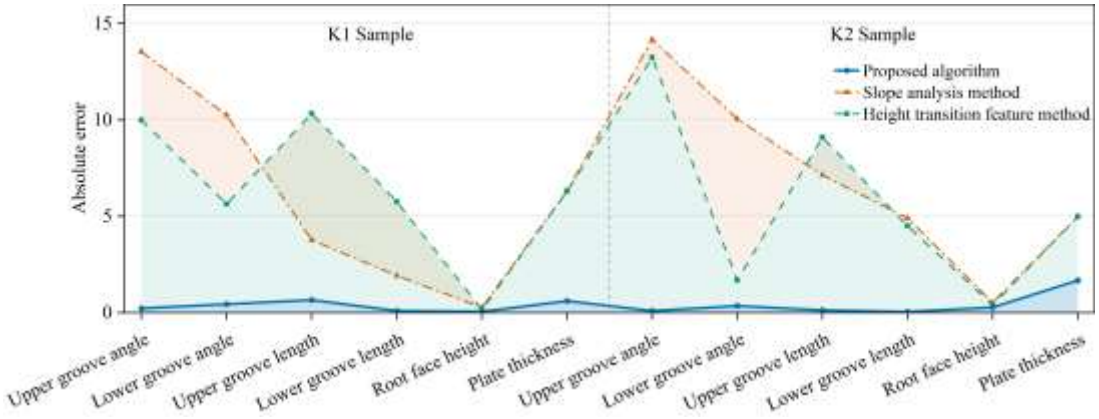


Figure 14 Error comparison of three algorithms on K-groove welds

Synthesizing the experimental results across all three weld types—I-groove, X-groove, and K-groove—the proposed algorithm achieves a mean MAE of 1.18 across all measurement parameters, representing an 81.8% accuracy improvement compared to the slope analysis method (mean MAE 6.47) and a 73.9% accuracy improvement compared to the height transition feature method (mean MAE 4.52), with an overall average measurement accuracy improvement of approximately 77.9%.

5 Conclusions

Addressing the extraction requirements for parameters of three types of butt weld joints—I-groove, X-groove, and K-groove—in ship manufacturing, an automatic parameter extraction algorithm based on laser scanning is proposed. Through the synergistic coordination of differentiated point cloud surface separation strategies, a universal parameter extraction module, and specialized extraction procedures, this algorithm achieves high-precision extraction of geometric parameters for multiple types of butt welds. The main conclusions are as follows:

(1) Differentiated surface separation for multi-type weld point clouds is achieved. For I-groove welds, automatic separation of left and right groove surfaces is accomplished based on DBSCAN density clustering; for X-groove and K-groove welds, a normal vector-based surface separation method is employed to accurately extract top and side surface point clouds. This strategy effectively adapts to the geometric differences of different groove structures, providing high-quality data support for precise weld parameter extraction.

(2) A universal parameter extraction module is constructed. Plate thickness extraction employs a percentile statistical filtering method, effectively suppressing the interference of surface noise and outliers; groove angle extraction adopts the endpoint method, which is less affected by local point cloud density fluctuations and possesses good measurement stability.

(3) High-precision parameter extraction for three weld types is achieved. For I-groove welds, the MAE of plate thickness and root gap is controlled within 0.7 mm; for X-groove welds, the groove angle MAE is controlled within 4°, and the MAE of root face height and plate thickness is controlled within 0.7 mm; for K-groove welds, the groove angle MAE is controlled within 0.5°, and the groove length MAE is controlled within 0.5 mm, satisfying the parameter accuracy requirements of ship welding processes.

(4) Comparative experiments validate the superiority of the proposed algorithm. Compared to the slope analysis method and height transition feature method, the proposed algorithm demonstrates higher measurement accuracy across all three weld types. With an 81.8% accuracy improvement over the slope analysis method, a 73.9% improvement over the height transition feature method, and an overall average measurement accuracy improvement of approximately 77.9%, the algorithm's robustness and broad applicability to both simple structures and complex double-sided multi-layer structures are fully demonstrated.

CRediT authorship contribution statement

Methodology, Yi Shen and Sheng Zhang; Validation, Yi Shen, Tao Ma and Yuanchao Lin; Writing - original draft, Sheng Zhang and Lijia Tao, Writing - review & editing, Sheng Zhang and Minxin Yuan.

Declaration of competing interest

The authors declare that they have no known competing financial interests or personal relationships that could have appeared to influence the work reported in this paper.

Acknowledgments

This research was funded by the High-tech Ship Scientific Research Project from the Ministry of Industry and Information Technology (CBG01N23-04-02) and the 2025 Industry–University Research Pre-research Fund Project of Zhangjiagang City (ZKCY2517).

References

[1] Wang Y Z, Xu F, Zhao J W, Li C, Chen Z, Xiao F (2025) Development trends of automation and intelligence in ship welding. Metal Working (Hot Working) (11): 8-12

[2] Zhou L J, Huang F, Chai C L, Kong J (2025) Design of structure and control system for ultrasonic welding industrial robot. Journal of Hebei University of Water Resources and Electric Engineering, 35(03): 14-21. https://doi.org/10.16046/j.cnki.issn2096-5680.2025.03.003.

[3] Guo Q, Yang Z, Xu J T, Jiang Y, et al (2024) Progress, challenges and trends on vision sensing technologies in automatic/intelligent robotic welding: State-of-the-art review. Robotics and Computer-Integrated Manufacturing, 89: 102767. https://doi.org/10.1016/j.rcim.2024.102767.

[4] Eren B, Demir M H, Mistikoglu S (2023) Recent developments in computer vision and artificial intelligence aided intelligent robotic welding applications. The International Journal of Advanced Manufacturing Technology, 126(9-10): 4763-4809. https://doi.org/10.1007/s00170-023-11456-4.

[5] Silva R H G, Galeazzi D, Schwedersky M B, et al (2021) An adaptive orbital system based on laser vision sensor for pipeline GMAW welding. Journal of the Brazilian Society of Mechanical Sciences and Engineering, 43(7): 358. https://doi.org/10.1007/s40430-021-03081-7.

[6] Yuan M X, Dai X L, Liu C, Sun H W, Wang L (2023) Extraction of ship weld seam feature parameters based on spatial position and contour line distance. Transactions of the China Welding Institution, 44(01): 84-92.

[7] Dai X L, Shen Y, Cao R X, Sun H W, Yuan M X (2022) Ship weld seam feature recognition based on triangulation and contour analysis. Science Technology and Engineering, 22(28): 12491-12498.

[8] Xue S C, Yang J, Ma X Y (2024) Weld seam feature recognition and feature parameter extraction method for complex welding parts. Journal of Chongqing University of Technology (Natural Science), 38(06): 149-154.

[9] Liu Y F (2025) Research on surface defect recognition method for mechanical parts based on laser vision sensing. Laser Journal, 46(10): 256-260.

[10] Xu F, He L, Hou Z, et al (2024) An automatic feature point extraction method based on laser vision for robotic multi-layer multi-pass weld seam tracking. The International Journal of Advanced Manufacturing Technology, 131: 5941-5960. https://doi.org/10.1007/s00170-024-13245-z.

[11] Baek D, Moon H (2025) Robust laser vision sensing technology for adaptive weld seam

tracking in shipbuilding automation. The International Journal of Advanced Manufacturing Technology, 139(3): 2003-2026. https://doi.org/10.1007/s00170-025-15896-y.

[12] Tang J J, Wei J, Sun L (2025) Research on welding point extraction algorithm for V-groove welds. Electronics Production, 33(05): 65-68.

[13] Liao P, Wang F H, Bu Y J (2024) Measurement method of three-dimensional morphological parameters for pressure pipeline welds based on deep feature point extraction. China Special Equipment Safety, 40(10): 15-22

[14] Zhou P, Peng R, Xu M, et al (2021) Path planning with automatic seam extraction over point cloud models for robotic arc welding. IEEE Robotics and Automation Letters, 6(3): 5002-5009. https://doi.org/10.1109/LRA.2021.3070828.

[15] Li C, Wang J T, Zhang J Y, Du C J (2026) Design of weld seam extraction method for H-shaped steel. Machinery Design & Manufacture (01): 94-98.

[16] Geng Y, Zhang Y, Tian X, et al (2022) A novel welding path planning method based on point cloud for robotic welding of impeller blades. The International Journal of Advanced Manufacturing Technology, 119(11-12): 8025-8038. https://doi.org/10.1007/s00170-021-08573-3.

[17] Yang L, Liu Y, Peng J Z, Liang Z Z (2020) A novel system for off-line 3D seam extraction and path planning based on point cloud segmentation for arc welding robot. Robotics and Computer-Integrated Manufacturing, 64: 101929. https://doi.org/10.1016/j.rcim.2019.101929.

[18] Zhang Y K, Jiang Y, Tian X C, Xu X L, et al (2023) A point cloud-based welding trajectory planning method for plane welds. The International Journal of Advanced Manufacturing Technology, 125(3-4): 1645-1659. https://doi.org/10.1007/s00170-022-10699-x.

[19] Zhou N, Jiang P, Jiang S, et al (2024) An identification and localization method for 3D workpiece welds based on the DBSCAN point cloud clustering algorithm. Journal of Manufacturing and Materials Processing, 8(6): 287. https://doi.org/10.3390/jmmp8060287.

[20] Singh P S, Nongsiej I M, Marboh V, Chutia D (2023) Three-dimensional point cloud segmentation using a combination of RANSAC and clustering methods. Current Science, 124(4): 467-475. https://doi.org/10.18520/cs/v124/i4/434-441.

[21] Xie T T, Chen H, Liu W Q, et al (2024) 3D surface segmentation from point clouds via quadric fits based on DBSCAN clustering. Pattern Recognition, 154: 110586. https://doi.org/10.1016/j.patcog.2024.110589.

[22] Hegedűs-Kuti J, Szőlősi J, Abonyi J, et al (2023) 3D scanner-based identification of welding defects—clustering the results of point cloud alignment. Sensors, 23(5): 2503. https://doi.org/10.3390/s23052503.